

## AgGaS<sub>2</sub> optical parametric oscillator continuously tunable from 3.9 to 11.3 μm

K. L. Vodopyanov,<sup>a)</sup> J. P. Maffetone, I. Zwieback, and W. Ruderman  
 INRAD, Inc., 181 Legrand Avenue, Northvale, New Jersey 07647

(Received 10 May 1999; accepted for publication 6 July 1999)

This is the experimental realization of a silver gallium sulfide (AgGaS<sub>2</sub>) optical parametric oscillator (OPO) with a wide mid-IR tuning range. The singly resonant angle-tuned AgGaS<sub>2</sub> type-II OPO was pumped by 1.06 μm pulses from a nanosecond Nd:YAG laser and yielded idler wave continuously tunable from 3.9 to 11.3 μm with a linewidth of 1 cm<sup>-1</sup>. The OPO threshold was 0.03 J/cm<sup>2</sup> corresponding to sub-MW/cm<sup>2</sup> pump intensity and sub-100 μJ pump energy. The slope and absolute quantum conversion efficiencies reached 41% and 22%, respectively. © 1999 American Institute of Physics. [S0003-6951(99)02435-3]

Chalcopyrite AgGaS<sub>2</sub> (AGS) crystal transmits light between 0.5 and 12 μm and demonstrates a high nonlinear optical coefficient combined with good mechanical properties. Its most remarkable characteristic, however, is that it is one of the few crystals<sup>1</sup> which can be pumped by commercially available 1 μm lasers to achieve phase-matched down-conversion into the λ > 5 μm region.

Difference frequency mixing (DFM) in AGS extending to λ ≥ 11 μm has been demonstrated in a number of studies with nano-,<sup>2-5</sup> pico-,<sup>6</sup> and femtosecond<sup>7,8</sup> pulses, as well as in the cw<sup>9,10</sup> regime. Seymour *et al.*<sup>3</sup> demonstrated that the long-wavelength limit of DFM output can be extended to as far as 18.3 μm (with weak yet detectable power)—beyond the two-phonon absorption band. A traveling-wave (superfluorescent) optical parametric generator based on AGS, pumped by 20 ps Nd:YAG laser pulses, with tunability over the range from 1.2 to 10 μm and a photon conversion efficiency of 0.1%–10% was demonstrated by Elsaesser *et al.*<sup>11</sup>

The first OPO based on AGS was reported in 1984 by Fan *et al.*<sup>12</sup> A type-I OPO was pumped by a Q-switched Nd:YAG laser (τ = 18 ns) and was tunable from 1.4 to 4 μm. The photon conversion efficiency was 16%. At λ > 4 μm the parametric oscillation threshold could not be reached because of surface damage to the crystal. This tuning range was extended (2.8–4.2 μm) in a recent work by Boon *et al.*<sup>13</sup>

A synchronously pumped singly resonant OPO with a signal wavelength near 1.3 μm and an idler wavelength near 5.5 μm was reported<sup>14</sup> with a cw actively mode-locked Nd:YAG laser as a pump source. A true cw OPO based on temperature-tuned, noncritically phase-matched AGS crystal, was recently reported by Douillet *et al.*<sup>15</sup> The subharmonic (3ω → 2ω + ω) doubly resonant OPO was pumped by a diode laser with λ = 845 nm at an input threshold power of 60 mW.

We report in this paper a singly resonant (SRO) OPO pumped by nanosecond λ = 1.06 μm pulses with a continuous tuning range of 3.9–11.3 μm, with 22% quantum conversion efficiency and extremely low pumping threshold. The OPO uses a single type-II phase-matched AGS crystal

which was grown at INRAD from the congruent melt by the horizontal gradient freeze technique. In order to eliminate optical scattering due to the Ga<sub>2</sub>S<sub>3</sub>-rich precipitates present in all melt-grown AGS crystals, the ingot was annealed at 900 °C in an excess of Ag<sub>2</sub>S.<sup>16</sup> The crystal was cut at θ = 45.1° to the optical z axis in the [100] direction (φ = 0), for type-II phase matching, and was 20 mm in length and 7 × 10 mm in cross section. Type II was chosen to (i) achieve narrower OPO linewidths and (ii) to maximize the effective second-order nonlinearity which is given by<sup>1</sup>

$$d_{\text{eff}} = d_{36} \sin \theta \sin 2\varphi \quad (\text{type I}), \quad (1)$$

$$d_{\text{eff}} = d_{36} \sin 2\theta \cos 2\varphi \quad (\text{type II}) \quad (2)$$

(here  $d_{36} = 12 \text{ pm/V}^1$  is the AGS nonlinear tensor component, and θ and φ are polar and azimuthal angles, respectively). Thus type-II phase matching with θ ~ 45° gives  $d_{\text{eff}} = 12 \text{ pm/V}$ , which is 25–30% higher than in the case of type I (θ ~ 52°), used in previous works.<sup>12,13</sup> The crystal surfaces were antireflection (AR) coated using ThF<sub>4</sub>/ZnSe dielectric layers so that the transmission at 1.06–1.46 μm varied between 97% and 99% (thus the crystal's bulk absorption can be estimated to be ≤ 0.005 cm<sup>-1</sup>). In the 4–8.5 μm range, transmission of the coated crystal was > 80%.

According to our SRO design, both OPO mirrors have high reflection (HR) at the signal (1.17–1.46 μm) wave. The input mirror M1 transmits, and the output mirror M2 reflects the pump at 1.06 μm (to achieve pump beam “recycling”). The Q factor for the idler should be kept small, thus at least one of the two mirrors should have high transmittance (HT) at 4–12 μm.

Figure 1 shows two configurations of SRO OPO, namely with one mirror transmissive and one reflective for the idler (configuration A) and both mirrors transmissive for the idler (configuration B). The parameters for configuration A are: M1 has T = 75% for the pump, R = 98%–100% for the signal, T ≈ 80% for the idler; M2(gold) has R ≈ 98% for all wavelengths. Configuration B: M1 has T = 75% for the pump, R = 98%–100% for the signal, T > 76% for the idler; M2 has R = 99.5% for the pump, R > 98.6% for the signal,

<sup>a)</sup>Electronic mail: kvodopyanov@inrad.com

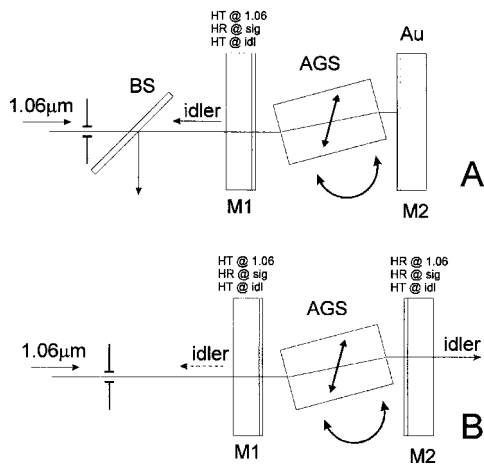


FIG. 1. Two configurations of SRO OPO based on AGS. Configuration A—with recycling both the pump and idler beams and configuration B—with recycling of the pump beam only. M1 and M2 are OPO mirrors; BS is a dichroic beam-splitter for extraction of the idler wave.

$T > 76\%$  for the idler. In both cases M1 and M2 were flat and spaced apart by 2.7 cm, just at the minimal distance allowed by the length of the AGS crystal (2 cm).

There are a few advantages of scheme A: (i) all the idler output goes in one direction, as compared to B where it goes in both directions; (ii) the idler wave generated in the first pass is reflected back, thus reducing the OPO threshold, and (iii) there is no walk-off of the output beam, due to the rotation of the AGS crystal.

We used as a pump an EO Q-switched Nd:YAG laser (Quantel YR580), which delivered pulses with up to 40 mJ per pulse at 10 Hz with a TEM<sub>00</sub> beam diameter  $\sim 1.6$  mm and pulse width of 12–100 ns (depending on the energy).

We measured the OPO spectrum by using a compact  $f = 15$  cm grating monochromator with a pyroelectric linear array (Spiricon LP-256-12) in the output focal plane. Figure 2 shows the calculated (solid line) and measured tuning curve for the AGS type-II OPO pumped at 1.064  $\mu\text{m}$ . We have found that the calculated dependence, based on dispersion relations by Roberts,<sup>17</sup> gives the best agreement with our experimental data.

From Fig. 2 one can also see that an idler beam tunability of 3.9–11.3  $\mu\text{m}$  was achieved with a single AGS crystal (the signal was tunable between 1.17 and 1.46  $\mu\text{m}$ , respectively). This is an unprecedented range for the AGS OPO: The longest wavelength achieved so far was 4.2  $\mu\text{m}$ .<sup>13</sup> The OPO linewidth was smaller than the spectral resolution of the monochromator, which we estimate to be 1.5–2  $\text{cm}^{-1}$ . The inset to Fig. 2 gives an OPO threshold dependence versus idler wavelength for configuration A. The curve is practically flat between 4 and 7  $\mu\text{m}$ ; at  $\lambda > 7$   $\mu\text{m}$ , however, the threshold starts rising, which correlates with the increasing AGS linear absorption at longer wavelengths. In addition, the threshold OPO intensity increases (as  $\sim \lambda_{\text{sig}} \lambda_{\text{idl}}$ ) when the OPO is tuned away from degeneracy, because of the decrease of gain increment.

Figure 3 represents the OPO threshold pump energy density (fluence) as a function of the pump pulse width for configuration A,  $\lambda_{\text{idl}} \approx 6$   $\mu\text{m}$ . The dashed curve is based on theoretical calculations, similar to Ref. 18 (we took into account that both pump and idler are reflected by the rear mirror M2).

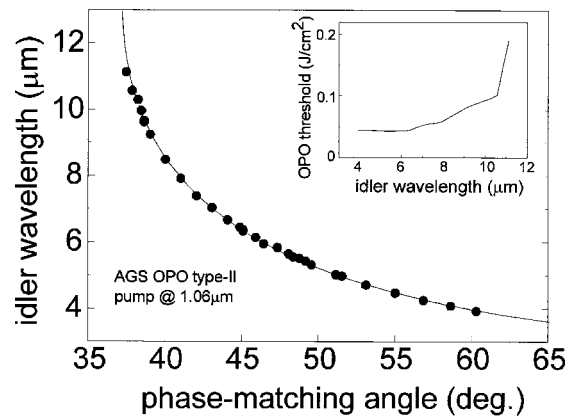


FIG. 2. AGS type-II OPO angular tuning curve (idler wave). Solid line—theoretical curve based on dispersion relations (Ref. 17). Inset: OPO threshold fluence as a function of the output idler wavelength.

We assumed  $d_{\text{eff}} = 12$  pm/V for AGS, and the roundtrip signal wave losses  $17 \pm 3\%$ . With some uncertainties of experimental parameters and relative simplicity of the model,<sup>18</sup> the calculated thresholds are surprisingly close (within 30%) to the experimental values. It is clear that one would expect the minimal threshold pump fluence at shorter pulse durations. For example, at  $\tau = 12$  ns the threshold fluence is as small as 0.03  $\text{J}/\text{cm}^2$ . Experimentally, we found that the threshold fluence (and intensity) remains the same when the beam size is reduced to  $w = 0.6$  mm (still, this is larger than the AGS crystal's birefringent walkoff distance of  $\sim 0.4$  mm at  $L = 2$  cm,  $\theta = 45^\circ$ ). The pump energy needed to achieve OPO operation at  $w = 0.6$  mm was as small as 85  $\mu\text{J}$ . Clearly, the minimal threshold intensity is achieved at longer pulse durations (e.g.,  $I_{\text{thr}} = 0.67$   $\text{MW}/\text{cm}^2$  at  $\tau = 100$  ns).

In Fig. 4, idler beam energy (at  $\lambda_{\text{idl}} \approx 6$   $\mu\text{m}$ ) is plotted as a function of pump energy. We used a Molelectron J4-05 pyroelectric energy meter and an InAs filter to cut off radiation with  $\lambda < 3.9$   $\mu\text{m}$ . The laser pulse width varied with energy but was typically 20–30 ns. The pump beam diameter was varied between 1.4 and 2.2 mm using a telescope and an iris diaphragm. A comparison of curves 1 and 2 shows that larger pump beam diameters gave higher output energies.

The conversion efficiency in configuration A reaches its maximum at about 2–3 pump thresholds. The laser-to-idler conversion (curve 1) was 4.9%, the quantum conversion efficiency 22%, and slope quantum conversion efficiency 39%. In configuration B the maximum conversion efficiency laser-

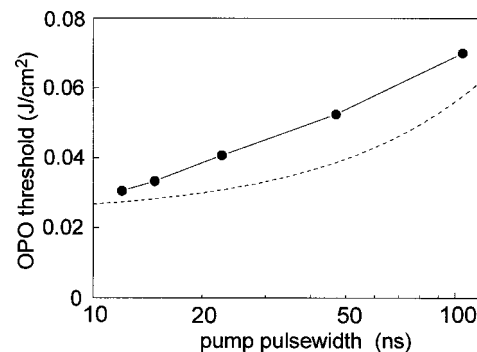


FIG. 3. OPO threshold fluence as a function of the pump pulse width (configuration A). Dashed curve—theoretical curve. The idler wavelength is around 6  $\mu\text{m}$ .

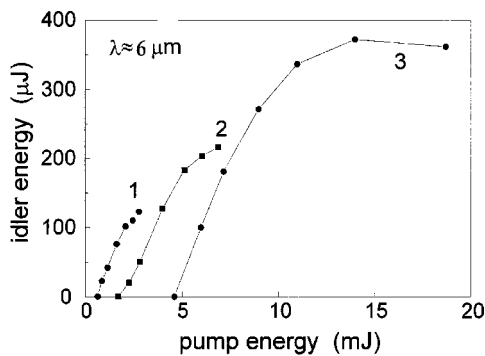


FIG. 4. OPO idler energy ( $\lambda \approx 6 \mu\text{m}$ ) plotted vs input laser energy. Curves 1 and 2 correspond to OPO configuration A and curve 3 to configuration B. Pump beam diameters are  $w = 1.4, 2.2,$  and  $1.6 \text{ mm}$  (curves 1, 2, and 3, respectively).

to-idler reached 3.1% (curve 3). This corresponds to quantum conversion efficiency of 18.2% and the slope efficiency 41.2%. The maximum idler energy was  $372 \mu\text{J}$ . These values are underestimated, however, because in configuration B we regarded only the idler radiation coming through the M2 mirror (Fig. 1), ignoring the idler coming in the opposite way.

A comparison of configurations A and B shows that A has smaller pumping thresholds (by a factor of  $\sim 5$ ) and higher absolute conversion efficiencies. However, scheme B is superior from the viewpoint of maximum extracted idler energy. The smaller absolute output in configuration A is apparently due to the backconversion process<sup>19</sup> (i.e., signal+idler  $\rightarrow$  pump) taking place during the second pass of the idler in the cavity.

The optical damage of the crystal surface within the OPO cavity occurs (with an exposure 3000 shots) at incoming pump energy density of  $0.2 \text{ J/cm}^2$ . We consider damage *fluence*, rather than *intensity*, to have physical sense at  $\tau < 100 \text{ ns}$ .<sup>18</sup> Interestingly, the optical damage of the surface of the AR coated crystal, which is not in the cavity, is 3 times higher ( $0.6 \text{ J/cm}^2$ ). This difference may be related to the presence, in the former case, of a strong resonated signal wave within the OPO cavity.<sup>12</sup> The OPO beam divergence (idler wave) was measured to be  $4.2 \text{ mrad}$  in the  $kz$  and  $8.4 \text{ mrad}$  in the orthogonal plane.

To demonstrate the feasibility of the OPO system for spectroscopic measurements and gas detection, as well as to estimate the OPO linewidth, we took absorption spectra of several gases with distinct rotational–vibrational features in the mid IR (e.g., CO, water vapor). Figure 5 compares the CO gas ( $p = 0.83 \text{ atm}$ ) absorption spectrum obtained with a Perkin–Elmer Fourier transform infrared (FTIR) spectrometer ( $2 \text{ cm}^{-1}$  resolution, upper curve) and with our OPO system (lower curve). One can see that the OPO provides better resolution of the fine structure. The inset to Fig. 5, shows one of the peaks at an expanded scale, from which we can estimate the OPO linewidth to be  $\sim 1 \text{ cm}^{-1}$ .

In conclusion, efficient frequency conversion of  $1.064 \mu\text{m}$  laser pulses into continuously tunable  $3.9\text{--}11.3 \mu\text{m}$  radiation with  $1 \text{ cm}^{-1}$  linewidth, up to  $0.4 \text{ mJ}$  per pulse, and 22% quantum conversion efficiency was achieved in a single-stage conversion process, with a type-II phase-matched OPO based on a  $\text{AgGaS}_2$  crystal. This is the longest

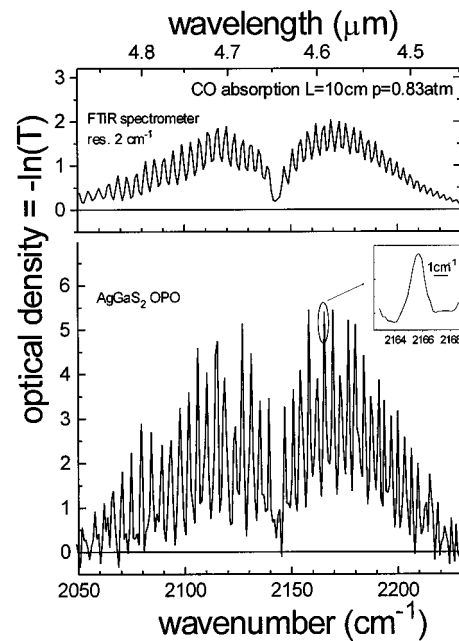


FIG. 5. CO absorption spectrum taken with a FTIR spectrometer ( $2 \text{ cm}^{-1}$  resolution, upper curve) and with the OPO system (lower curve).

wavelength OPO pumped at  $1 \mu\text{m}$ . The remarkably low threshold pump energies ( $< 100 \mu\text{J}$ ) make this OPO system extremely promising when used with existing commercial laser diode-pumped Nd lasers delivering millijoule nanosecond pulses with a repetition rate  $\sim 1 \text{ kHz}$ .

The authors acknowledge the support of the National Science Foundation by a Phase-I SBIR Grant No. DMI-9561306. The assistance of Feruz Ganihanov in the experiment is gratefully acknowledged.

<sup>1</sup>V. G. Dmitriev, G. G. Gurzadyan, and D. N. Nikogosyan, *Handbook of Nonlinear Optical Crystals* (Springer, Berlin, 1997), pp. 136–175.

<sup>2</sup>D. C. Hanna, V. V. Rampal, and R. C. Smith, *Opt. Commun.* **8**, 151 (1973).

<sup>3</sup>R. J. Seymour and F. Zernike, *Appl. Phys. Lett.* **29**, 705 (1976).

<sup>4</sup>K. Kato, *IEEE J. Quantum Electron.* **QE-20**, 698 (1984).

<sup>5</sup>S. Haidar, K. Nakamura, E. Niwa, K. Masumoto, and H. Ito, *Appl. Opt.* **38**, 1798 (1999).

<sup>6</sup>H. J. Krause and W. Daum, *Appl. Phys. B: Photophys. Laser Chem.* **56**, 8 (1993).

<sup>7</sup>P. Hamm, C. Lauterwasser, and W. Zinth, *Opt. Lett.* **18**, 1943 (1993).

<sup>8</sup>B. Golubovic and M. K. Reed, *Opt. Lett.* **23**, 1760 (1998).

<sup>9</sup>V. Petrov, C. Rempel, K. P. Stolberg, and W. Schade, *Appl. Opt.* **37**, 4925 (1998).

<sup>10</sup>D. Lee, T. Kaing, and J. J. Zondy, *Appl. Phys. B: Lasers Opt.* **67**, 363 (1998).

<sup>11</sup>T. Elsaesser, A. Seilmeier, W. Kaiser, P. Koidl, and G. Brandt, *Appl. Phys. Lett.* **44**, 383 (1984).

<sup>12</sup>Y. X. Fan, R. L. Eckardt, R. L. Byer, R. K. Route, and R. S. Feigelson, *Appl. Phys. Lett.* **45**, 313 (1984).

<sup>13</sup>P. P. Boon, W. R. Fen, C. T. Chong, and X. B. Xi, *Jpn. J. Appl. Phys., Part 1* **36**, L1661 (1997).

<sup>14</sup>E. C. Cheung, K. Koch, and G. T. Moore, *Opt. Lett.* **19**, 631 (1994).

<sup>15</sup>A. Douillet and J. T. Zondy, *Opt. Lett.* **23**, 1259 (1998).

<sup>16</sup>I. Zwieback, J. Maffetone, and W. Ruderman, Final Report No. PL-TR-96-1028, Air Force Material Command, Kirtland AFB, 1996.

<sup>17</sup>J. N. Roberts, *Appl. Opt.* **35**, 4677 (1996).

<sup>18</sup>S. J. Brosnan and R. L. Byer, *IEEE J. Quantum Electron.* **QE-15**, 415 (1979).

<sup>19</sup>R. L. Byer and R. L. Herbst, in *Nonlinear Infrared Generation*, Topics in Applied Physics Vol. 16, edited by Y. R. Shen (Springer, Berlin, 1977), p. 121.